2017

Towards Internet of Underground Things in Smart Lighting: A Statistical Model of Wireless Underground Channel

Abdul Salam
University of Nebraska-Lincoln, salama@purdue.edu

Mehmet C. Vuran
University of Nebraska-Lincoln, mcvuran@cse.unl.edu

Suat Irmak
University of Nebraska-Lincoln, suat.irmak@unl.edu

Towards Internet of Underground Things in Smart Lighting: A Statistical Model of Wireless Underground Channel

Abdul Salam and Mehmet C. Vuran

Cyber-Physical Networking Laboratory
Department of Computer Science & Engineering
University of Nebraska-Lincoln, Lincoln, NE 68588
Email: {asalam, mcvuran}@cse.unl.edu

Suat Irmak

Department of Biological Systems Engineering
University of Nebraska-Lincoln, Lincoln, NE 68583
Email: sirmak2@unl.edu

***Abstract*—The Internet of Underground Things (IOUT) has many applications in the area of smart lighting. IOUT enables communications in smart lighting through underground (UG) and aboveground (AG) communication channels. In IOUT communications, an in-depth analysis of the wireless underground channel is important to design smart lighting solutions. In this paper, based on the empirical and the statistical analysis, a statistical channel model for the UG channel has been developed. The parameters for the statistical tapped-delay-line model are extracted from the measured power delay profiles (PDP). The PDP of the UG channel is represented by the exponential decay of the lateral, direct, and reflected waves. The developed statistical model can be used to generate the channel impulse response, and precisely predicts the UG channel RMS delay spread, coherence bandwidth, and propagation loss characteristics in different conditions. The statistical model also shows good agreement with the empirical data, and is useful for tailored IOUT solutions in the area of smart lighting.**

I. Introduction

In Internet of Underground Things (IOUT) [16], [19], sensors and communication devices, both buried and over the air (OTA), forms an internet of things for real time communications and sensing of the environment in which these are deployed. IOUTs have many applications in areas including environment and infrastructure monitoring [2], [3], [10], [13], [23], border patrol [4], and precision agriculture [1], [6], [16], [17], [18], [19], [20], [25].

A potential application of the IOUT is in the area of smart lighting [9], [8], [22], where cables are buried underground for control of intelligent lighting systems. The overview of the smart lighting IOUT system architecture is shown in Fig. 1. The IOUT architecture connects underground and aboveground communication devices and sensors using two types of the wireless channel, i.e., underground (UG), and above-ground (AG). The smart lighting IOUT applications include road lighting, lamp posts, airport runway lighting, household driveway and garage illumination, and garden decoration. In these applications, over-the-air (OTA) channel can be eliminated completely, and all communication can be carried out through IOUT UG and AG channels. A smart lighting

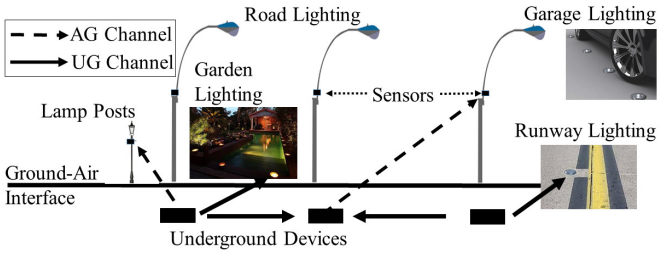

Fig. 1: Overview of smart lighting IOUT system architecture.

IOUT architecture has many advantages over the OTA: 1) the need to have a wired underground communication network can be completely eliminated, 2) by bringing the communication devices underground, complexity of cabling to power aboveground devices is reduced, and 3) interference and spectrum congestion issues are avoided. In smart lighting IOUT, through real time sensing of the environment, all illumination needs of the environment can be met effectively with high energy efficiency. This IOUT approach also results in improved smart lighting solutions and cost reduction of the system deployment.

A detailed characteristic of the wireless UG channel is vital for design of such IOUT communication systems. In [20], we have conducted a detailed empirical characterization of the wireless UG channel in different soils under different soil moisture conditions through both the testbed and field experiments. The goal of the measurement campaign [20], and the corresponding model is to produce a reliable channel model which can be used in heterogeneous IOUT deployments. Thus, we have considered several possible scenarios with extensive measurements taken over the period of many years. In [20], the time domain characteristics of channel such as RMS delay spread, coherence bandwidth, and multipath power gains are analyzed empirically. The analysis of the power delay profile (PDP) validated the three main components of the UG channel, i.e. direct, reflected, and lateral waves. Underground communication challenges are discussed in [20].

In this paper, we develop a statistical model for the wireless UG channel based on the empirical evaluations presented in

978-1-5090-4429-0/17/$31.00

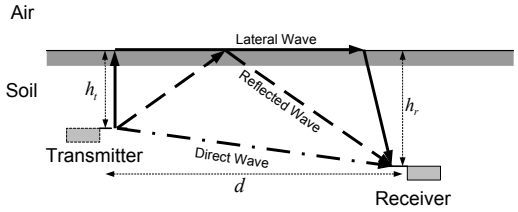

Fig. 2: L, D, and R-Wave in the UG channel [5].

[20]. The statistical model is based on the analysis of the properties of the power delay profiles measured in different soils under different water content levels in the indoor testbed [20] and field settings. To engineer an IOUT communication system for smart lighting, a statistical model of propagation in the wireless underground channel is useful in optimizing system performance, designing tailored modulated/coding schemes, and in end-to-end capacity analysis. Moreover, the developed statistical model can be used to generate the channel impulse response, and precisely predicts the UG channel RMS delay spread, coherence bandwidth, and propagation loss characteristics in different UG conditions. The aim of this paper is to focus on the statistical analysis and the modeling of the UG channel, rather than on the measurements and experiments, for it we refer the reader to [20]. The rest of the paper is organized as follows: the related work is discussed in Section II. Background is discussed in Section III. The statistical channel impulse response model is developed in Section IV. In Section V, model evaluations are performed numerically. Empirical validation of the developed statistical impulse response model is done in Section VI. Paper is concluded in Section VII.

II. Related Work

Smart lighting is an emerging field [8], [9], and there exist only few architectures. Use of the IOUT communications in this field has not been investigated before. Intelligent light control using sensor networks has been proposed in [22], however, it does not use the UG channel. An OTA intelligent lighting control architecture has been proposed in [7].

Smart lighting IOUT UG wireless channels (UG and AG) requires detailed characterization. In [26], we have developed a 2-wave model without consideration of the lateral wave. In [23], a model for underground communication in mines and road tunnels has been developed but it cannot be applied to IOUT due to dissimilarities in wave propagation mechanisms of tunnels and soil. We have also developed a closed-form path loss model using lateral waves in [5] but channel impulse response and statistics cannot be captured through this simplified model. Magnetic induction (MI) [12], [24], is another wave propagation mechanism in the underground communications. In MI, received signal strength decreases rapidly with distance and high data rates can not be achieved. Moreover, communications cannot be carried out if sender receiver coils are at right angles. Long wavelengths of the MI channel limit the network architecture scalability. To the best of our knowledge, this is the first statistical model for the wireless underground channel based on an empirical campaign [20] conducted to characterize the channel impulse response of UG channel for IOUT communications.

III. Background

The analysis of the experimental data [20] reveals that direct, lateral, and reflective wave are the three major components in the underground communications. In Fig. 2, the L, D and R-Wave in the UG channel is shown. The UG channel impulse response is expressed as [20]:

$$\begin{aligned} h_{ug}(t) = & \sum_{i=0}^{L-1} \alpha_{li} e^{j\theta_{li}} \delta(t-\tau_l-\tau_{li}) \\ + & \sum_{j=0}^{D-1} \alpha_{dj} e^{j\theta_{dj}} \delta(t-\tau_d-\tau_{dj}) \\ + & \sum_{k=0}^{R-1} \alpha_{rk} e^{j\theta_{rk}} \delta(t-\tau_r-\tau_{rk}) \ , \end{aligned} \tag{1}$$

where phases θ_{li}, θ_{dj}, and θ_{rk} are represented by statistically independent random variables with uniform distribution over [0,2π).

Arrival time of each of these three components are denoted by τ_d, τ_r and τ_l for direct, reflected and lateral waves, respectively. α_d, α_r and α_l represents the maximum multipath gains of each of the three components, and D, R, and L are the maximum number of multipath within each component. Therefore, delays and multipath gains in each of the three components becomes τ_{di}, τ_{rj}, τ_{lk}, and α_{di}, α_{rj} and α_{lk}, where i, j, and k indices are used to denote the multipaths in each component. The first multipath within each component is set such that $\tau_{d0} = \tau_d$, $\tau_{r0} = \tau_r$, and $\tau_{l0} = \tau_l$. Arrival times of these components are modeled deterministically based on the speed of wave propagation in the soil medium. Speed of the wave in soil is given as $S = c/n$, where $c = 3\text{x}10^8$ m/s is the speed of light, n is the refractive index of soil $n = \sqrt{\sqrt{\epsilon'^2 + \epsilon''^2} + \epsilon'/2}$, and ϵ' and ϵ'' are the real and imaginary parts of the relative permittivity of the soil. Arrival time of each of the three components, in nanoseconds, is calculated as follows [20]:

$$\tau_l = 2 \times (\delta_s/S) + (\delta_a/c), \tag{2}$$

$$\tau_d = (\delta_s/S), \tag{3}$$

$$\tau_r = 2 \times (\delta_s/S), \tag{4}$$

where τ_d, τ_r and τ_d are arrival times of the direct, reflected and lateral waves, respectively, δ_s is distance travel by wave in soil, S is speed of wave in soil, and c is the speed of light ($3\text{x}10^8$ m/s).

IV. The Statistical Model

To model the wireless underground channel, our approach follows the standard OTA modeling approaches described in [15], [21], [11], and [27], with modifications due to unique nature of wireless propagation in the underground channel. Based on the measurement analysis, following assumptions are made:

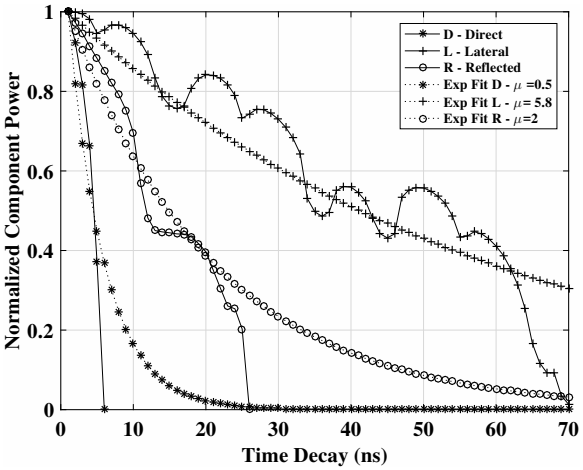

Fig. 3: Decay of three components with exponential decay fit.

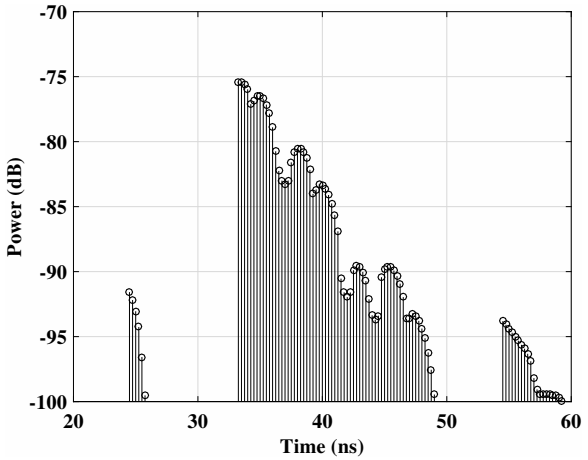

Fig. 4: A realization of wireless underground channel impulse response

1) Correlation among multipath components at different delays in the lateral, reflected, and direct component is very small and negligible for all practical purposes. However multipaths within each component are affected by the strongest path and hence are correlated. Therefore, the tap-delay-lines are assumed uniformly spaced within each component.

2) At the receiver, phases are completely random with uniform distribution over [0, 2π).

To keep model tractable, arrival rate of delays within each component is kept constant, and amplitudes of these multipaths in each component are statistically independent. This helps in modeling the physical characteristics of the UG channel and provide ease of analysis without losing insight into delay statistics. The order of the arrival of the lateral, direct, and reflected component depends upon the burial depth, distance between transmitter-receiver (T-R), because the path traversal through soil and air exhibits different wave propagation speeds depending on the soil characteristics, and soil moisture level. Only for the T-R distances less than 50 cm, direct component arrives first, and as the distances increases, the lateral component reaches at the receiver first due to higher propagation speed in the air medium. Due to significant differences in speed of the three components in soil and air mediums, no component overlap is observed, and power of multipaths (gain) within each components decays before the arrival of the next component. Moreover, in our measurements, there were not any significant detectable components observed beyond the 100 ns time delay.

Next, statistics of amplitudes α_{li}, α_{dj}, α_{rk} at delays τ_{li}, τ_{di}, τ_{ri} for lateral, direct, and reflected waves, respectively, are derived. In Fig. 3, mean amplitudes of a profile have been shown at $50\,\mathrm{cm}$ distance with exponential decay fit. Analysis of the measurement data shows that gains of multipaths within each component follow the exponential decay. Therefore, the path amplitudes of the three components are modeled as decaying exponentials within each component. The multipath amplitudes calculated from the arrival time τ_L, decay rate γ_L, and amplitude α_L of the lateral component. It is given as [21]:

$$\alpha_{li} = \alpha_{l0} e^{-(i-\tau_L)/\gamma_L} \ \forall \ i > \tau_l \ and \ i < \tau_l + L. \quad (5)$$

The α_{dj} for the direct component is obtained from the arrival time τ_D, decay rate γ_D, and amplitude α_D of the direct component. It is expressed as:

$$\alpha_{dj} = \alpha_{d0} e^{-(j-\tau_D)/\gamma_D} \ \forall \ j > \tau_d \ and \ j < \tau_d + D. \quad (6)$$

Similarly, for the reflected component, α_{rk} is given as:

$$\alpha_{rk} = \alpha_{r0} e^{-(k-\tau_R)/\gamma_R} \ \forall \ k > \tau_r \ and \ k < \tau_d + R. \quad (7)$$

Gain of first multipath is denoted as α_{d0}, α_{l0}, and α_{r0}. These multipaths within each components are calculated as follows [5]:

$$\begin{aligned}
\alpha_{d0} &= P_t + 20\log_{10}\lambda_s - 20\log_{10} r_1 - 8.69\alpha_s r_1 \\
&\quad -22 + 10\log_{10} D_{rl} \ , \\
\alpha_{r0} &= P_t + 20\log_{10}\lambda_s - 20\log_{10} r_2 - 8.69\alpha_s r_2 \\
&\quad +20\log_{10}\Gamma - 22 + 10\log_{10} D_{rl} \ , \\
\alpha_{l0} &= P_t + 20\log_{10}\lambda_s - 40\log_{10} d - 8.69\alpha_s (h_t + h_r) \\
&\quad +20\log_{10} T - 22 + 10\log_{10} D_{rl} \ ,
\end{aligned} \quad (8)$$

where P_t is the transmitted power, Γ and T are reflection and transmission coefficients [5], respectively, r_2 is the length of the reflection path, $r_1 = \sqrt{(h_t - h_r)^2 + d^2}$, $r_2 = \sqrt{(h_t + h_r)^2 + d^2}$, where h_t and h_r are transmitter and receiver burial depth, and λ_s is the wavelength in soil [17].

In the statistical model, exponential decay is justified because the time delay depends on the travel paths, and the path gains are affected by the soil. Therefore gains of the successive multipaths depends on the delay of those multipaths. It is also important to note that, in addition to the soil moisture, the multipath gains α_{li}, α_{dj}, α_{rk} are also impacted by soil type. For example, in sandy soils path gains are much higher due to lower attenuation as compared to the silt loam and silty clay loam soils due to the less water absorption of EM waves in sandy. This is attributed to the low water holding capacity of sandy soils. However, soil type impact on multipaths gains α_{li}, α_{dj}, α_{rk} does not require separate modeling in (5) - (7), therefore, it is captured in the main lateral, direct, and reflected components α_{l0}, α_{d0}, α_{r0} and is propagated to α_{li}, α_{dj}, α_{rk} in (5) - (7) due to their dependence on α_{l0}, α_{d0}, α_{r0}.

TABLE I: The impulse response model parameters.

Parameter	Description	Model	Values
S	Speed of wave in soil [20]	C/η	$C = 3 \times 10^8$
η	Refraction Index [20]	$\eta = \sqrt{\sqrt{\epsilon'^2 + \epsilon''^2} + \epsilon'/2}$	ϵ', ϵ''
ϵ'	Real part of relative permittivity of the soil [14]	$\epsilon'_s = \begin{cases} 1.15\Big[1 + \rho_b/\rho_s\left(\epsilon_s^\delta - 1\right) + (m_v)^{\nu'}(\epsilon'_{fw})^\delta - \\ \quad m_v\Big]^{1/\delta} - 0.68 \qquad 0.3\,\text{GHz} \le f \le 1.4\,\text{GHz}\,, \\ \Big[1 + \rho_b/\rho_s\left(\epsilon_s^\delta - 1\right) + (m_v)^{\nu'}(\epsilon'_{fw})^\delta - m_v\Big]^{1/\delta} \\ \qquad\qquad 1.4\,\text{GHz} \le f \le 18\,\text{GHz}\,, \end{cases}$	S = Sand in %, C= Clay in %, $\delta = 0.65$, $\nu' = 1.2748 - 0.519S - 0.152C$, $\nu'' = 1.33797 - 0.603S - 0.166C$ ϵ'_{fw}, ϵ''_{fw}
ϵ''	Imaginary part of relative permittivity of the soil [14]	$\epsilon''_s = \Big[(m_v)^{\nu''}(\epsilon''_{fw})^\delta,\Big]^{1/\delta}$	
ϵ'_{fw}	Real part of relative permittivity of the free water [14]	$\epsilon'_{fw} = e_{w\infty} + \frac{\epsilon_{w0} - \epsilon_{w\infty}}{1 + (2\pi f \tau_w)^2}$	$\epsilon_{w\infty} = 4.9$ is the limit of ϵ'_{fw} when $f \to \infty$, ϵ_{w0} is the static dielectric constant for water, τ_w is the relaxation time for water, and ϵ_0 is the permittivity of free space. At room temperature,$2\pi\tau_w = 0.58 \times 10^{-10} s$ and $\epsilon_{w0} = 80.1$, effective conductivity, δ_{off}
ϵ''_{fw}	Imaginary part of relative permittivity of the free water [14]	$\epsilon''_{fw} = \frac{2\pi, f\tau_w(\epsilon_{w0} - \epsilon_{w\infty})}{1 + (2\pi, f\tau_w)^2} + \frac{\delta_{eff}}{,2\pi\epsilon_0 f}\frac{(\rho_s - \rho_b)}{\rho_s m_v}$	
δ_{eff}	Effective conductivity of soil [14]	$\delta_{eff} = \begin{cases} 0.0467 + 0.2204\rho_b - 0.4111S + 0.6614C \\ \qquad 0.3\,\text{GHz} \le f \le 1.4\,\text{GHz}\,. \\ -1.645 + 1.939\rho_b - 2.25622S + 1.594C \\ \qquad 1.4\,\text{GHz} \le f \le 18\,\text{GHz} \end{cases}$	ρ_b is bulk density
τ_d	Arrival time of direct component	$\tau_d = (\delta_s/S)$	S is speed of wave in soil
τ_r	Arrival time of reflected component	$\tau_r = 2 \times (\delta_s/S)$	S is speed of wave in soil
τ_l	Arrival time of reflected component	$\tau_l = 2 \times (\delta_s/S) + (\delta_a/c)$	S is speed of wave in soil C is speed of wave in air
α_{d0}, α_{r0}, α_{l0},	Gains of the three main components	$\alpha_{d0} = P_t + 20\log_{10}\lambda_s - 20\log_{10} r_1 - 8.69\alpha_s r_1$ $-22 + 10\log_{10} D_{rl}$ $\alpha_{r0} = P_t + 20\log_{10}\lambda_s - 20\log_{10} r_2 - 8.69\alpha_s r_2$ $+20\log_{10}\Gamma - 22 + 10\log_{10} D_{rl}$ $\alpha_{l0} = P_t + 20\log_{10}\lambda_s - 40\log_{10} d - 8.69\alpha_s(h_t + h_r)$ $+20\log_{10} T - 22 + 10\log_{10} D_{rl}$, See also analysis from [20, Table VI].	μ and σ
α_{di}, α_{rj}, α_{lk}	Path amplitudes of the three components	$\alpha_{li} = \alpha_{l0} e^{-(i-\tau_L)/\gamma_L}\ \forall,\ i > \tau_l\ and\ i < \tau_l + L$ $\alpha_{dj} = \alpha_{d0} e^{-(j-\tau_D)/\gamma_D}\ \forall,\ j > \tau_d\ and\ j < \tau_d + D$ $\alpha_{rk} = \alpha_{r0} e^{-(k-\tau_R)/\gamma_R}\ \forall,\ k > \tau_r\ and\ k < \tau_d + R$	

Next, number of significant paths are determined. Number of multipaths L, D, and R in each of the components are determined by setting a gain threshold (paths within 30 dB from peak). Multipath generation in a particular component is stopped once the path amplitude in that bin falls below the threshold value. This results in larger number for the sandy soils, and lower number of multipaths for silt loam, and silty clay loam soils which is also in good agreement with empirical observations. Moreover, this number being an indicator of the channel spread, also depends on the soil moisture. Higher soil moisture leads to lower spread, and on the other hand lower soil moisture decrease attenuation, which leads to emergence of higher number of multipaths falling above the threshold value and higher number of multipaths. A realization of underground channel impulse response model is shown in Fig. 4. Model parameters are shown in Table I.

Up to this point, α_l, α_d, α_r are calculated based on the delays within lateral, reflected, and direct components which depends on the exponential decay of multipath with respect to the main path gain in each component. This is a good realization of physical measurements. However, if we normalize the path gains with each components by average of these gains such that $\alpha_{li}/\bar{\alpha_{li}}$, $\alpha_{dj}/\bar{\alpha_{dj}}$, and $\alpha_{rk}/\bar{\alpha_{rk}}$, then, these amplitudes become independent of the delays to which these

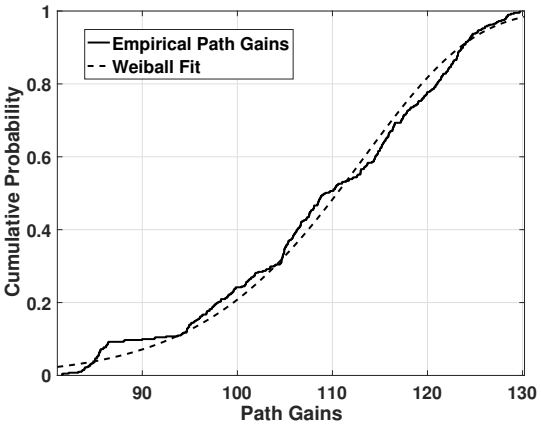

Fig. 5: Amplitude gains with Weibull distribution fit.

are associated [21]. Accordingly, a commutative distribution of path gains normalized through this process is shown in Fig. 5, which follows the Weibull probability distribution.

V. Model Evaluation

Model parameters required to evaluate the statistical model are summarized in the Table I. In the numerical evaluation, first, we need to find the the α_{li}, α_{dj}, α_{rk} and their associated delays τ_{li}, τ_{di}, τ_{ri}. After generating the delays and amplitudes of these three components, other impulse response parameters are found and compared with the measurement data. An algorithm to generate UG channel impulse response is shown in Algorithm 1.

Simulation algorithm takes soils parameters such as soil type, and soil moisture as input and calculates the arrival times of the direct, reflected, and lateral components, τ_d, τ_r and τ_d by using the (4) to (3). Based on the soil type, peak power gains τ_{d0}, τ_{r0}, τ_{l0}, are determined from the [20, Table VI]. Model parameters for peak amplitude, delays, and number of multipaths statistics for direct, lateral and reflected components for three soil types are given in [20, Table VI].

Different statistical parameters computed from the measurement data, and the channel model numerical evaluations are compared in Table II. UG channel is evaluated numerically using the the statistical model. The RMS delay spread and

Algorithm 1 UG Channel Impulse Response Simulation

1: *Initialization* :
2: Input soil parameters
3: Obtain the soil moisture level
4: **BEGIN**
5: Generate decay exponents for the lateral, direct, and reflected components
6: Determine the arrival time
7: Calculate the first multipath gain of each of the three components
8: Generate multipaths and impulse response
9: **END**

TABLE II: Validation of impulse response model parameters.

Impulse Response Parameter	Measured	Modeled
RMS Delay Spread (τ_{rms})	45.52 ns	38.84 ns
Coherence Bandwidth	439 kHz	514 kHz

the coherence bandwidth parameters are derived and compared with the parameters obtained through experimental data. Model prediction error for RMS delay spread is 14.67%, and for the the coherence bandwidth, it is 14.08%. It can be observed that the difference in predicted and measured values, which is due to model uncertainty and observational error, is less than 15%. Overall, the developed statistical model shows a good agreement with the empirical data, and statistics of the coherence bandwidth and RMS delay spread prove the validity of the statistical model.

VI. Empirical Validation

A good statistical model should be able to simulate the empirical measurements with higher accuracy. Moreover, simulated response must have the same characteristics as of the measurements results. In this section, arrival of multipath components is validated with experiments conducted in the indoor testbed (Fig. 6) [20]. Moreover, the shape of the PDP is presented and physical interpretations are discussed.

Based on (4), (4) and (3), the speed of the wave in all three soils is found by calculating the refractive indices n based on particle size distribution and classification of soils given in ([20, Table I]). The results of these calculations are shown in ([20, Table V]). In Fig. 7, a measured PDP for a silt loam at $40\,\mathrm{cm}$ depth is compared with a schematic representation of the 3-wave model for T-R separation of $50\,\mathrm{cm}$. Analysis of arrival time of three components reveals that for 50 Cm distance and all burial depths, lateral waves arrive later than the direct wave except for the 10 Cm depth where lateral wave reaches the receiver first. It can be observed that measurement data shows a strong agreement with the model.

From Fig. 7, it can also be observed that lateral component is the strongest component than the direct and reflected components. This is because direct and reflected components are spherical waves, propagating radially outward from the antenna, whereas, the lateral component is, initially, a plane wave that travels upward from the source to the boundary, then horizontally as a cylindrical wave, and subsequently travels backward as a plane wave from boundary to the point of observation.

The proposed model is applicable to heterogeneous smart lighting scenarios. However, in order to improve the model,

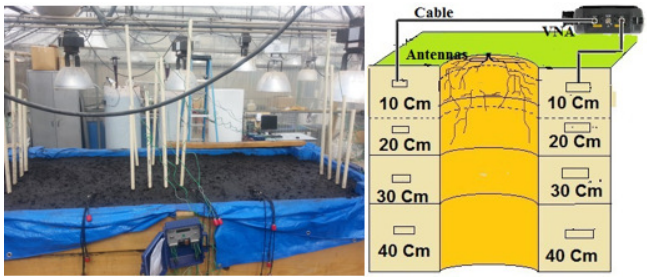

(a)
Fig. 6: The indoor testbed [20].

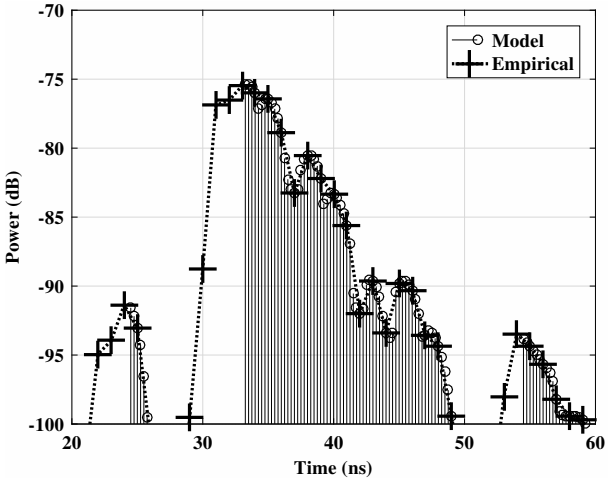

Fig. 7: Comparison of model and empirical impulse response in silt loam.

it is important to further understand the specialized smart lighting requirements for a particular environment IOUT deployment. Accordingly, tailored sensing, control, and communication strategies can be exploited.

VII. Conclusion

In this paper, we presented an application of the IOUT to the smart lighting. We analyzed the UG channel data, collected through extensive measurements in the indoor and a field testbed. Accordingly, a statistical impulse response model of underground channel in IOUT communications is developed and validated through empirical evaluations. Power delay profile data from the measured delay profiles is analyzed and model statistics are developed. The model is capable of generating the wireless underground channel impulse response for different soils under different soil moisture conditions. It also accurately captured the delay spread and coherence bandwidth statistics. This statistical model serves as an important characterization tool for the UG channel, and gives practical insight for design of a smart lighting IOUT communications system.

VIII. Acknowledgments

This work is supported in part by NSF grants NSF CNS-1619285, NSF DBI-1331895, and NSF CNS-1423379.

References

[1] P. Abouzar, D. G. Michelson, and M. Hamdi, "Rssi-based distributed self-localization for wireless sensor networks used in precision agriculture," *IEEE Transactions on Wireless Communications*, vol. 15, no. 10, pp. 6638–6650, Oct 2016.

[2] T. E. Abrudan, O. Kypris, N. Trigoni, and A. Markham, "Impact of rocks and minerals on underground magneto-inductive communication and localization," *IEEE Access*, vol. 4, pp. 3999–4010, 2016.

[3] I. F. Akyildiz and E. P. Stuntebeck, "Wireless underground sensor networks: Research challenges," *Ad Hoc Networks Journal (Elsevier)*, vol. 4, pp. 669–686, July 2006.

[4] I. F. Akyildiz, Z. Sun, and M. C. Vuran, "Signal propagation techniques for wireless underground communication networks," *Physical Communication Journal (Elsevier)*, vol. 2, no. 3, pp. 167–183, Sept. 2009.

[5] X. Dong and M. C. Vuran, "A channel model for wireless underground sensor networks using lateral waves," in *Proc. of IEEE Globecom '11*, Houston, TX, December 2011.

[6] X. Dong, M. C. Vuran, and S. Irmak, "Autonomous precision agricultrue through integration of wireless underground sensor networks with center pivot irrigation systems," *Ad Hoc Networks (Elsevier)*, 2012.

[7] P. Elejoste, I. Angulo, A. Perallos, A. Chertudi, I. J. G. Zuazola, A. Moreno, L. Azpilicueta, J. J. Astrain, F. Falcone, and J. Villadangos, "An easy to deploy street light control system based on wireless communication and led technology," *Sensors*, vol. 13, no. 5, pp. 6492–6523, 2013.

[8] A. K. Gopalakrishna, T. Ozcelebi, A. Liotta, and J. J. Lukkien, *Statistical Inference for Intelligent Lighting: A Pilot Study*. Cham: Springer International Publishing, 2015, pp. 9–18.

[9] A. K. Gopalakrishna, T. Ozcelebi, J. J. Lukkien, and A. Liotta, "Relevance in cyber-physical systems with humans in the loop," *Concurrency and Computation: Practice and Experience*, vol. 29, no. 3, 2017.

[10] H. Guo and Z. Sun, "Increasing the capacity of magnetic induction communication using mimo coil-array," in *2016 IEEE GLOBECOM*, Dec 2016, pp. 1–6.

[11] H. Hashemi, "Impulse response modeling of indoor radio propagation channels," *IEEE Journal on Selected Areas in Communications*, vol. 11, no. 7, pp. 967–978, Sep 1993.

[12] S. Kisseleff, I. F. Akyildiz, and W. H. Gerstacker, "Magnetic induction based simultaneous wireless information and power transfer for single information and multiple power receivers," *IEEE Transactions on Communications*, vol. PP, no. 99, pp. 1–1, 2017.

[13] G. Liu, Z. Wang, and T. Jiang, "Qos-aware throughput maximization in wireless powered underground sensor networks," *IEEE Transactions on Communications*, vol. 64, no. 11, pp. 4776–4789, Nov 2016.

[14] N. Peplinski, F. Ulaby, and M. Dobson, "Dielectric properties of soil in the 0.3–1.3 ghz range," *IEEE Transactions on Geoscience and Remote Sensing*, vol. 33, no. 3, pp. 803–807, May 1995.

[15] T. Rappaport, S. Seidel, and K. Takamizawa, "Statistical channel impulse response models for factory and open plan building radio communicate system design," *IEEE Transactions on Communications*, vol. 39, no. 5, pp. 794–807, May 1991.

[16] A. Salam and M. C. Vuran, "Impacts of soil type and moisture on the capacity of multi-carrier modulation in internet of underground things," in *Proc. of the 25th ICCCN 2016*, , Hawaii, USA, Aug 2016 (Best Student Paper Award).

[17] A. Salam and M. C. Vuran, "Smart underground antenna arrays: A soil moisture adaptive beamforming approach," Department of Computer Science and Engineering, University of Nebraska-Lincoln, Tech. Rep. TR-UNL-CSE-2017-0001, January 2017.

[18] A. Salam and M. C. Vuran, "Smart underground antenna arrays: A soil moisture adaptive beamforming approach," in *Proc. IEEE INFOCOM 2017*, Atlanta, USA, May 2017.

[19] A. Salam and M. C. Vuran, "Wireless underground channel diversity reception with multiple antennas for internet of underground things," in *Proc. IEEE ICC 2017*, Paris, France, May 2017.

[20] A. Salam, M. C. Vuran, and S. Irmak, "Pulses in the sand: Impulse response analysis of wireless underground channel," in *Proc. IEEE INFOCOM 2016*, San Francisco, USA, Apr. 2016.

[21] A. Saleh and R. Valenzuela, "A statistical model for indoor multipath propagation," *IEEE Journal on Selected Areas in Communications*, vol. 5, no. 2, pp. 128–137, February 1987.

[22] V. Singhvi, A. Krause, C. Guestrin, J. H. Garrett, Jr., and H. S. Matthews, "Intelligent light control using sensor networks," in *Proceedings of the 3rd CenSys*, ser. SenSys '05, 2005, pp. 218–229.

[23] Z. Sun and I. Akyildiz, "Channel modeling and analysis for wireless networks in underground mines and road tunnels," *IEEE Transactions on Communications*, vol. 58, no. 6, pp. 1758–1768, June 2010.

[24] X. Tan, Z. Sun, and I. F. Akyildiz, "Wireless underground sensor networks: Mi-based communication systems for underground applications." *IEEE Antennas and Propagation Magazine*, vol. 57, no. 4, pp. 74–87, Aug 2015.

[25] M. Vuran, X. Dong, and D. Anthony, "Antenna for wireless underground communication," Dec. 27 2016, US Patent 9,532,118. [Online]. Available: https://www.google.com/patents/US9532118

[26] M. C. Vuran and I. F. Akyildiz, "Channel model and analysis for wireless underground sensor networks in soil medium," *Physical Communication*, vol. 3, no. 4, pp. 245–254, December 2010.

[27] M. Win and R. Scholtz, "Characterization of ultra-wide bandwidth wireless indoor channels: a communication-theoretic view," *IEEE Journal on Selected Areas in Communications*, vol. 20, no. 9, pp. 1613–1627, Dec 2002.